Journal of Hazardous Materials 166 (2009) 88–93

Contents lists available at ScienceDirect

Journal of Hazardous Materials

journal homepage: www.elsevier.com/locate/jhazmat

Research Article

Investigation of a basic dye removal from aqueous solution onto chemically modified Unye bentonite

Erdal Eren*

Department of Chemistry, Ahi Evran University, Faculty of Arts and Science, 40100 Kırşehir, Turkey

ARTICLE INFO

Article history:
Received 30 July 2008
Received in revised form 1 November 2008
Accepted 3 November 2008
Available online 17 November 2008

Keywords:
Dye adsorption
Clay
Kinetics
X-ray diffraction
Bentonite

ABSTRACT

The adsorption behavior of crystal violet (CV^+) from aqueous solution onto magnesium-oxide coated bentonite (MCB) sample was investigated as a function of parameters such as initial CV^+ concentration, contact time and temperature. The Langmuir, and Freundlich adsorption models were applied to describe the equilibrium isotherms. The Langmuir monolayer adsorption capacity of MCB were estimated as 496 mg/g. The pseudo-first-order, pseudo-second-order kinetic and the intra-particle diffusion models were used to describe the kinetic data and rate constants were evaluated. The values of the energy (E_a), enthalpy ($\Delta H^{\neq}$) and entropy of activation ($\Delta S^{\neq}$) were 56.45 kJ/mol, 53.90 kJ/mol and −117.26 J/mol K, respectively, at pH 6.5.

1. Introduction

Dyes are generally classified in three categories: (a) anionic: direct, acid and reactive dyes; (b) cationic: all basic dyes and (c) nonionic: disperse dyes. Basic dyes can be applied to wool, silk and leather [1]. This group dyes can cause allergic dermatitis, skin irritation, cancer, and mutations. There are several methods for dye removal, such as adsorption, oxidation–ozonation, coagulation, coagulation–flocculation and biological methods. Adsorption process provides an attractive alternative treatment to other removal techniques because it is more economical and readily available. A lot of non-conventional, low-cost and easily obtainable adsorbents have been tested for basic dye removal such as clay minerals [2–6], biomaterial [7], activated carbons [8,9], and solid wastes [10–12].

Bentonite is a clay mainly composed of montmorillonite known as a 2/1 type aluminosilicate. Its crystalline structure presents an alumina octahedral between two tetrahedral layers of silica. The isomorphous substitution of Al^{3+} for Si^{4+} in the tetrahedral layer and Mg^{2+} for Al^{3+} in the octahedral layer results in a net negative surface charge on the clay. This negative charge is balanced by the presence of exchangeable cations (Na^+, Ca^{2+}, etc.) in the lattice structure. These cations could be exchanged by the organic cation by the ion exchange mechanism. Besides the contribution of ion exchange sites, the sites satisfied with adsorption of single cation and neutral adsorption sites on montmorillonite surfaces may contribute to the adsorption of dye cations [13].

Since there is a huge deposit of Unye (Turkey) bentonite, there is a great potential for its utilization in wastewater treatment. The current annual production of Unye bentonite is estimated about 45,000 tons. The aim of this paper is to examine the effectiveness and of the magnesium oxide-coated bentonite (MCB) in removing crystal violet (CV^+) from aqueous solution and determine adsorption characteristics of CV^+ onto the MCB sample. In fact, several investigators have suggested applications for different oxides in water and wastewater treatment [14–18]. But, bentonite has never been used as a support for magnesium oxide for dye removal from wastewater. The effects of dye concentration and solution temperature were studied to understand the adsorption process. Desorption experiments were also carried out by CV^+-loaded MCB in different solutions such as KCl in water and ethanol.

2. Experimental

2.1. Materials

The preparation of RB is already discussed in previous work [19]. RB had a mineral composition of 76% montmorillonite, 8% quartz, 12% dolomite and 4% other minerals. Whitness was found to be 85%. RB was composed of 62.70% SiO_2, 20.10% Al_2O_3, 2.16% Fe_2O_3, 2.29%CaO, 3.64% MgO, 0.27%, Na_2O, 2.53% K_2O, 0.21% TiO_2, P_2O_5% 0.02. The ignition loss of the RB at 1273 K was also found to be 6.1%. The cation exchange capacity (CEC), determined

* Tel.: +90 386 2114525.
E-mail address: eeren@ahievran.edu.tr.

0304-3894/$ – see front matter © 2008 Elsevier B.V. All rights reserved.
doi:10.1016/j.jhazmat.2008.11.011

Nomenclature

RB	raw bentonite
CV^+	crystal violet
C_e	equilibrium concentration of the adsorbate in the solution (mg/L)
D_p	average pore diameter
k_1	pseudo-first-order rate constant of adsorption (1/h)
k_2	pseudo-second-order rate constant of adsorption (g/mg min)
k_i	intra-particle diffusion rate constant (g/mg $min^{1/2}$)
K_L	constant that represents the energy or net enthalpy of adsorption (L/mg)
K_F	Freundlich constant indicative of the adsorption capacity of the adsorbent (mg/g)
m	mass of adsorbent (g/L)
MCB	magnesium oxide coated bentonite
n	experimental constant indicative of the adsorption intensity of the adsorbent
q_e	amount of adsorbate removed from aqueous solution at equilibrium (mg/g)
q_t	amount of adsorbate sorbed on the sorbent surface at any time *t* (mg/g)
q_m	mass of adsorbed solute completely required to saturate a unit mass of adsorbent (mg/g)
S_{BET}	the BET surface area
S_{ext}	external surface area (including only mesopores)
S_{mic}	micropores surface area
t	reaction time (min)
V_t	total pore volume

with triethanolamine-buffered $BaCl_2$ solution (c = 0.1 M) followed by a reexchange with aqueous $MgCl_2$ solution (c = 0.1 M), is of 0.65 mmol/g [20].

2.1.1. Preparation of MCB

Magnesium nitrate and sodium hydroxide were mainly used in the modification of RB to enhance the adsorption capacity of RB. 20 g of RB were immersed in sufficient 2.0 M sodium hydroxide and temperature of the reaction mixture was maintained at 90 °C for 4 h. The base activated RB was dispersed into 150 ml of 0.1 M $Mg(NO_3)_2$ aqueous solution. 300 ml of 0.1 M NaOH aqueous solution was added slowly with a drop rate 1 ml/hour. The obtained powder was rinsed with 0.01 M HCl aqueous solution to remove the excess $Mg(OH)_2$ precipitated on the outher surface of the clay and further washed with deionized water. Then, this sample was heated for 4 h in air at 700 K. The thermal treatment of mixed solids in air at 700 K led to the formation of MgO [21,22]

2.2. Dye adsorption measurement

Adsorption of CV^+ (C.I.No. 42555, dye content, ~90%, chloride salt, obtained from Reidel-de Haen) was carried out by a batch technique to obtain equilibrium data. The experiments of adsorption equilibrium and kinetics were carried out as similarly described before [19]. The adsorption capacity of CV^+ molecules adsorbed per gram adsorbent (mg/g) was calculated using the equation:

$$q_e = (C_0 - C_e)\frac{V}{m} \quad (1)$$

where q_e is the equilibrium concentration of CV^+ on the adsorbent (mg/g), C_0 the initial concentration of the CV^+ solution (mg/L), C_e the equilibrium concentration of the CV^+ solution (mg/L), m the mass of adsorbent (g), and *V* the volume of CV^+ solution (L).

The equilibrium data have been analyzed using Langmuir and Freundlich isotherms and the characteristics parameters for each isotherm have been determined [22,23]. In order to investigate the adsorption mechanism, the constants of adsorption and intra-particle diffusion rate were determined using equations of Lagergren [24], Ho and McKay [25], and Weber and Morris [26]. The rate constants (k_2) of the pseudo-second-order model were adopted to calculate the activation energy of the adsorption process using the Arrhenius equation [27]. In order to study the effect of solution temperature on the kinetic process of dye adsorption were determined using the Eyring equation [27]. A clear review of these equations and their applications is in literature [19]. These equations are given in Appendix A.

Desorption experiments were carried out by immersing the MCB loaded with dye in 50 mL of desorption solution for 4 h at room temperature. In the batch desorption process, different desorption solutions were tested and the mixtures of KCl in ethanol/water solutions (e.g. 0.5 M KCl in 50% ethanol or 0.5 M KCl in water). The dye concentration in desorption solution was analyzed spectrophotometrically and the calibration curves for different desorption solutions were obtained.

The structure of the dye studied is shown below:

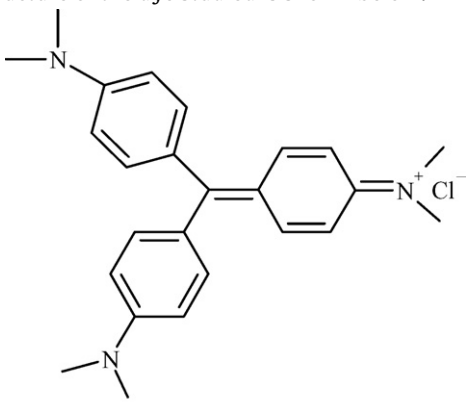

Crystal Violet

2.3. Characterization methods

The mineralogical compositions of the RB and MCB samples were determined from the X-ray diffraction (XRD) patterns of the products taken on a Rigaku 2000 automated diffractometer using Ni filtered CuKα radiation.

3. Results and discussion

3.1. Material characterization

The XRD patterns of RB and MCB samples were presented in Fig. 1. For the XRD pattern of RB, one reflection was observed in the region $2^\circ < 2\theta < 8^\circ$ (Fig. 1a). This corresponds to the 5.76° (2θ) value from which the interlamellar distance was found to be 15.33 Å. After heat treatment at 700 K the position of d_{001} peak shifted from 15.33 Å in RB to 14.31 Å in MCB (Fig. 1b), which was accompained by a intensity decrease from 100% to 9.4% (Table 1). This result indicates that the intercalated structure of pillared clay is not maintained during the coating process. Because, it is known that pillaring process causes an expansion in the interlayer spacing [28]. Heating at 700 K produced a decrease of basal spacing from 15.33 to 14.31 Å,

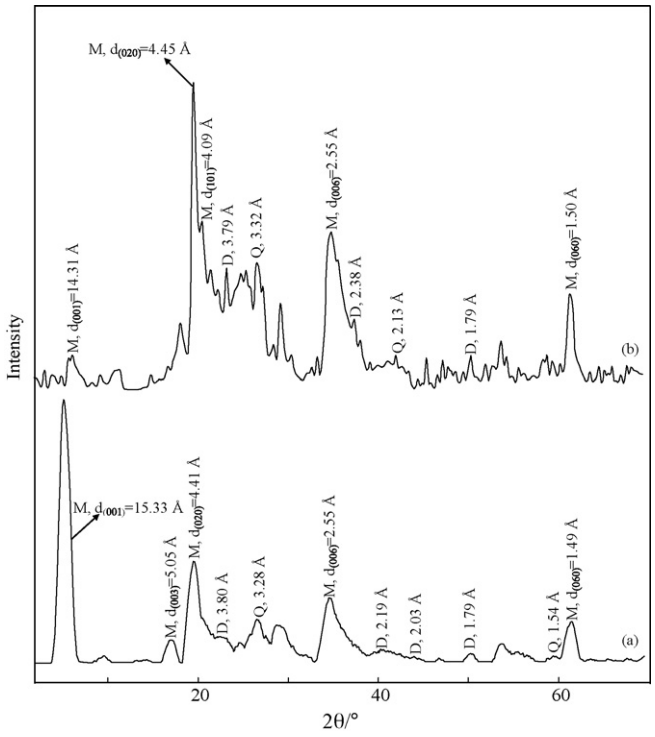

Fig. 1. The X-ray diffraction patterns of the RB (A) and MCB (B) samples (M: montmorillonite).

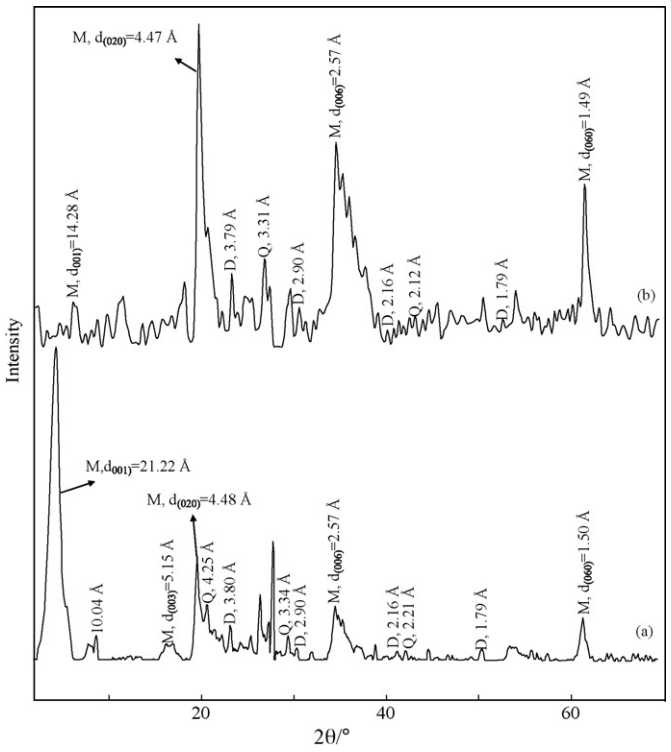

Fig. 2. The X-ray diffraction patterns of the dye-loaded RB (A) and MCB (B) samples (M: montmorillonite, Q: quartz, D: dolomite).

attributable to the removal of interlayer water. Subtraction of the thickness of the 2:1 layer of 9.60 Å yields an interlayer separation of 4.71 Å in MCB. The XRD results also show that modification has caused structural changes in the bentonite sample. Modification has affected mainly the 0 0 1 reflection; the intensities of the 0 0 1 and 0 0 6 reflections have been reduced, while the intensities of the 0 2 0 and 0 6 0 reflections has been increased significantly by the modification process (Table 1). The XRD peak intensities for MCB is less than those for some of the peaks for RB. Normally, the XRD intensity is closely related with the crystallinity and particle size of the sample [29]. Considering that MgO could be highly dispersed in the internal structure of montmorillonite, it is inferred that the decrease of peak intensity in MCB is due to the fine particle size distribution. This may be the cause for the broader and less intense peaks of the MCB sample compared with that for RB.

Modification of the RB yielded d_{101} reflection at 4.05 Å ($2\theta = 21.68^\circ$), which is absent in the RB. Appearance of new reflection indicate the formation of expansible phases and interlamellar expansion [30]. The formation of a new structure was illustrated by the peak appearing at lower <6.17° in the XRD pattern of the MCB. The new peaks situated at lower 2θ value (<6.17°) were likely to appear because of agglomeration of the MCB sheets [31]. MCB sample displays an increase of the background in the interval between 20° and 30°. The d_{003} reflection of RB at 5.05 Å ($2\theta = 17.52^\circ$) disappeared after modification process.

The adsorption of CV^+ on the RB led to significant increase in the basal spacing of the host material, from 15.33 to 21.22 Å, and new shoulders appeared (Fig. 2a). The basal spacing of the CV^+ adsorbed RB is consistent with a bilayer to pseudo trilayer arrangement of adsorbed CV^+ [32–34].

3.2. Equilibrium isotherm models

The equilibrium data for CV^+ adsorption on MCB were fitted to Langmuir equation: an equilibrium model useful in understanding the type of adsorbent/adsorbate interactions (physical or chemical) involved. Linear plots of C_e/q_e versus C_e (not shown) were employed to determine the value of q_m (mg/g) and K_L (L/mg). The Langmuir monolayer adsorption capacity of MCB was estimated as 496 mg/g (Table 2).

The equilibrium data also fitted to Freundlich equation, a fairly satisfactory empirical isotherm can be used for non-ideal adsorption. K_F relates the multilayer adsorption capacity and n intensity of adsorption, which varies with the heterogeneity of the adsorbent [35–37]. A relatively $n \ll 1$ indicates that adsorption intensity is favorable over the entire range of concentrations studied, while

Table 1
d-spacing and I/I_0 values of reflections for bentonite samples.

Reflection	RB		RB/CV^+		MCB		MCB/CV^+	
	d (Å)	I/I_0	d (Å)	I/I_0	d (Å)	I/I_0	d (Å)	I/I_0
d_{001}	15.33	100	21.22	100	14.31	9.4	14.28	9.7
d_{003}	5.05	8	5.15	6	–	–	–	–
d_{020}	4.42	34	4.48	34	4.45	100	4.47	100
d_{101}	–	–	–	–	4.05	5.9	–	–
d_{006}	2.55	21	2.57	18	2.55	13	2.57	53
d_{060}	1.49	13	1.50	14	1.49	41	1.49	40

Table 2
Langmuir and Freundlich isotherm parameters for the adsorption of CV^+ onto MCB.

Sample	Langmuir isotherm constants			Freundlich isotherm constants		
	q_m (mg/g)	K_L (L/mg)	R^2	n	K_f ($mg^{(1-1/n)} L^{1/n}/g$))	R^2
MCB	496	0.52	0.969	6.31	243	0.988

Table 3
Adsorption results of basic dyes from the literature by various adsorbents.

Adsorbent	Q_m (mg/g)	Ref. nos.
Kaolin	47.27	[6]
Raw bentonite	131	[19]
Manganese oxide coated raw bentonite	457	[19]
Phosphoric acid activated carbon	60.42	[39]
Sulphuric acid activated carbon	85.84	[39]
MCM-41	236.64	[40]
Saw dust	341	[41]
Activated carbon prepared from waste apricot	57.80	[42]
Polymer	12.9	[43]
Activated carbon prepared from waste apricot	32.89	[44]
MCM-22	48.96	[45]
Palygorskite	57.8	[46]
Jute fiber carbon	27.999	[47]
MCB	496	In this study

$n > 1$ means that adsorption intensity is favorable at high concentrations but much less at lower concentrations [37,38]. The Freundlich adsorption capacity (K_F) was found to be 243 for the MCB sample. The high value of K_F is indicate the high adsorption capacity of MCB. In the adsorption system, n value is 6.31 which indicate that adsorption intensity is favorable over the entire range of concentrations studied.

The adsorption capacities of the adsorbents for the removal of CV^+ have been compared with those of other adsorbents reported in literature and the values of adsorption capacities have been presented in Table 3. The values reported in the form of monolayer adsorption capacity. The experimental data of the present investigation are comparable with the reported values [6,19,39–47]. The value of maximum adsorption capacity (q_m) for MCB calculated from the Langmuir isotherm in this study is much higher than that of those reported in the literature. The uptake of CV^+ on manganese oxide coated raw bentonite has Langmuir monolayer capacity $q_m = 457$ mg/g [19]. This value shows that relative to manganese oxide coated bentonite, magnesium oxide coated bentonite have a higher affinity for CV^+ (Table 3). Adsorption of CV^+ on sulphuric acid activated carbon follows the Langmuir isotherm model with an adsorption capacity of 85.84 mg/g [39]. Lee et al. [40] have reported a Langmuir monolayer capacity of 236.64 mg/g at for CV^+ adsorption onto MCM-41. Langmuir adsorption capacity for CV^+ adsorption on saw dust has been shown to be 341 mg/g by Chakraborty et al. [41].

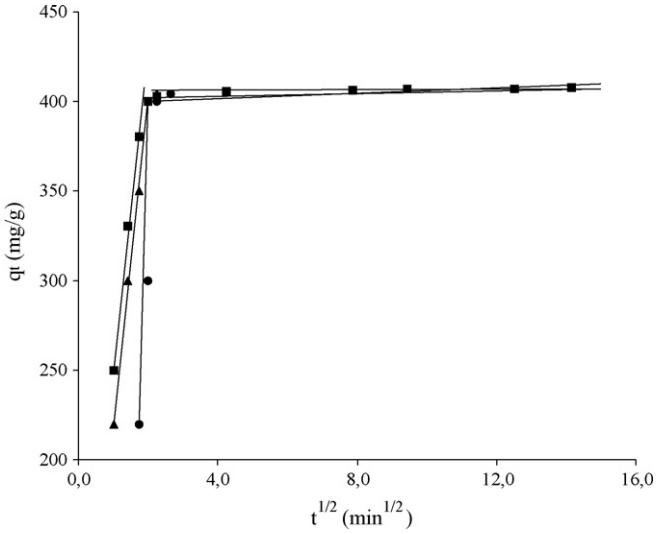

Fig. 3. Amount of dye adsorbed vs. $t^{1/2}$ for intraparticle diffusion of CV^+ by MCB sample at different temperatures, 295 K; squares, 308 K; triangles, 318 K; circles. $C_0 = 410$ mg/L, initial pH 6.5, and $m = 2$ g/L.

3.3. Adsorption kinetics

Table 4 lists the results of the rate constant studies for different initial dye concentrations by the pseudo-first-order and pseudo-second-order models. The correlation coefficient, R^2 for the pseudo-second-order adsorption model has high value (>98%), and its calculated equilibrium adsorption capacity ($t_{e,cal}$) is consistent with experimental data. These facts suggest that the pseudo-second-order adsorption mechanism is predominant. As given in Table 4, when the CV^+ initial concentration increases from 150 to 410 mg/L, the rate constant, k_2, decreases from 1.60×10^{-3} to 1.23×10^{-3} mg/g min. This is due to after the initial stage of adsorp-

Table 4
Kinetic parameters for the adsorption of CV^+ onto MCB sample at different initial dye concentrations.

C_0 (mg/L)	Pseudo-first order model		Pseudo-second order model		
	R_1^2	k_1 (min^{-1})	R_2^2	$q_{e,2}$ (mg/g)	k_2 ($\times 10^3$ g/mg min)
150	0.692	0.20	0.934	194	1.60
410	0.617	0.27	0.999	454	1.23

Table 5
Kinetic parameters for the adsorption of CV^+ onto MCB sample at different temperatures.

Temp. (K)	Pseudo-first order model	Pseudo-second order model				Intra-particle diffusion model			
	R_1^2	R_2^2	$q_{e,cal}$ (mg/g)	k_2 ($\times 10^3$ g/mg min)	$k_{i,1}$ (mg/g $min^{1/2}$)	$R_{i,1}^2$	$k_{i,2}$ (mg/g $min^{1/2}$)	$R_{i,2}^2$	C (mg/g)
295	0.617	0.972	454	1.23	206	0.825	0.17	0.788	47
308	0.600	0.997	421	4.06	156	0.970	0.16	0.934	73
318	0.602	0.998	416	6.33	127	0.897	0.15	0.896	139

Contact time 200 min, $C_0 = 410$ mg/L, initial pH 6.5, and $m = 2$ g/L.

Table 6
Thermodynamic parameters for the adsorption of CV^+ onto MCB.

Temp. (K)	k_2 ($\times 10^3$ g/mg min)	E_a (kJ/mol)	R^2	$\Delta H^{\neq}$ (kJ/mol)	$\Delta S^{\neq}$ (J/mol)	$\Delta G^{\neq}$ (kJ/mol)	$T_{av}\,\Delta S^{\neq}$ (kJ/mol)
295	1.23					88.50	
308	4.06	56.45	0.974	53.90	−117.26	90.02	−36.62
318	6.33					91.13	

Contact time 200 min, C_0 = 410 mg/L, initial pH 6.5, and m = 2 g/L.

tion, the remaining vacant surface sites are difficult to be occupied due to repulsive forces between the CV^+ molecules on the MCB surface.

The intra-particle diffusion plots for the effect of temperature to the adsorption of CV^+ onto MCB were shown in Fig. 3. From this figure, it was observed that there are two linear portions. The calculated $k_{i,1}$ and $k_{i,2}$ values for different solution temperatures are given in Table 5. The $k_{i,1}$ and $k_{i,2}$ express diffusion rates of the different stages in the adsorption. The changes of $k_{i,1}$ and $k_{i,2}$ could be attributed to the adsorption stages of the exterior surface and interior surface. At the beginning, the CV^+ was adsorbed by the exterior surface of MCB particle, so the adsorption rate was very fast. When the adsorption of the exterior surface reached saturation, the CV^+ entered into the MCB particle and was adsorbed by the interior surface of the MCB particle. The values of the intercept (C in Table 5) also give an idea about the boundary layer thickness: the larger the intercept, the greater is the boundary layer effect. Namely, any increase in the value of C indicates the abundance of solute adsorbed on boundary layer. The results of this study demonstrated increasing the temperature promoted the boundary layer diffusion effect.

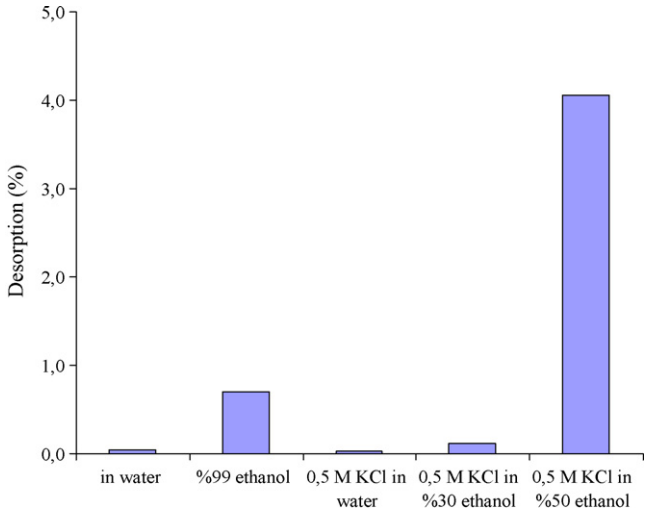

Fig. 4. Batch desorption results of CV^+. Contact time 200 min, T = 295 K, C_0 = 410 mg/L, initial pH 6.5, and m = 2 g/L.

3.4. Thermodynamic parameters

The activation energy of CV^+ adsorption onto MCB was calculated using Arrhenius equation, since the pseudo-second-order kinetic model was suitable in describing the kinetic data for CV^+ adsorption onto MCB. The activation energy is 56.45 kJ/mol at pH 6.5 (Table 6). This value is consistent with the values in the literature where the activation energy was found to be 33.96 kJ/mol for the adsorption of maxilon blue GRL onto sepiolite [27], 33.35 kJ/mol for the adsorption of reactive dye (Procion Red MX-5B) on carbon nanotubes [48], 47.5 kJ/mol for the adsorption of lac dye onto silk [49], and 37.21 kJ/mol for the adsorption of basic brown 1 on poly(*c*-glutamic acid) [50]. The magnitude of the activation energy yields information on whether the adsorption is mainly physical or chemical. Wu [48] suggested that the physisorption process normally had activation energy of 5–40 kJ/mol, while chemisorption had a higher activation energy (40–800 kJ/mol). Also, low activation energy values (<42 kJ/mol) indicate diffusion control processes and the higher activation energy values (>42 kJ/mol) indicate chemically controlled processes, due to the temperature dependence of the pore diffusivity is relatively weak [51].

The high $\Delta H^{\neq}$ value for CV^+ shows that the interactions between CV^+ and MCB are strong. On the other hand, the positive values of $\Delta G^{\neq}$ and $\Delta H^{\neq}$ indicate the presence of an energy barrier in the adsorption process. The negative $\Delta S^{\neq}$ value reflects that no significant change occurs in the internal structure of MCB during adsorption of CV^+. Furthermore, the negative sign of the entropy means that things are finally more organized than in the start. The values of $T_{av}\,\Delta S^{\neq}$ can be calculated from the experimental data where T_{av} represents the average values of the range of temperature used for adsorption studies. It is found be $\Delta H^{\neq} < -T_{av}\,\Delta S^{\neq}$. This means, although contribution of $\Delta H^{\neq}$ are not negligible, the influence of entropy is more remarkable than that of the enthalpy in activation. The values of free energies of activation can be calculated, respectively, which are also listed in Table 6. For all adsorption systems, $\Delta G^{\neq} > 0$, which means the adsorption of CV^+ dye on RB is not spontaneous and need additional energy to complete.

3.5. Desorption studies

In order to probe further into the mechanistic aspects of the cationic dye adsorption onto MCB, desorption studies were conducted. The batch CV^+ desorption results are displayed in Fig. 4. The use of aqueous KCl and ethanol solutions for CV^+ desorption is ineffective. Very low desorption of CV^+ (<5%) with these solutions suggests that some complex formation takes place between the active sites of MCB and the cationic group of CV^+. In Fig. 4, the mixtures of aqueous ethanol solutions with KCl did not greatly improve the CV^+ desorption. These results indicate that the CV^+ were bound onto the MCB through electrostatic interaction binding force. Ethanol did not help to breaking this binding interaction. The above stated observations were well corroborated with the adsorption equilibrium and kinetic data discussed earlier.

4. Conclusions

The amount of dye adsorbed was found to vary with initial CV^+ concentration, contact time and temperature. The maximum adsorption capacity of CV^+ for MCB sample is higher than that for raw material. From this result, it is appeared that the surface properties of raw bentonite could be improved upon modification of magnesium-oxide. It was found that the kinetics of the adsorption of CV^+ onto bentonite sample at different initial concentrations was the best described by the pseudo-second-order model. Based on the results, it was concluded that MCB had a significant potential for removing basic dye from wastewater using adsorption method.

Appendix A

Model	Equation
Langmuir isotherm	$C_e/q_e = C_e/q_m + 1/K_L q_m$
Freundlich isotherm	$\log q_e = \log K_F + (1/n)\log C_e$
First-order mechanism	$\log(q_e - q_t) = \log q_e - (k_1/2.303)t$
Pseudo-second-order mechanism	$t/q_t = (1/h) + (1/q_e)t$
Intraparticle diffusion	$q_t = k_i t^{1/2} + c$
Arrhenius	$\ln k_2 = \ln A - E_a/RT$
Eyring	$\ln(k_2/T) = \ln(k_b/h) + \Delta S^{\neq}/R - \Delta H^{\neq}/RT$

References

[1] E.N. El Qada, S.J. Allen, G.M. Walker, Adsorption of basic dyes from aqueous solution onto activated carbons, Chem. Eng. J. 135 (2008) 174–184.
[2] S.S. Tahir, N. Rauf, Chemosphere, Removal of a cationic dye from aqueous solutions by adsorption onto bentonite clay 63 (2006) 1842–1848.
[3] M. Turabik, Adsorption of basic dyes from single and binary component systems onto bentonite: simultaneous analysis of Basic Red 46 and Basic Yellow 28 by first order derivative spectrophotometric analysis method, J. Hazard. Mater. 158 (2008) 52–64.
[4] C. Bilgiç, Investigation of the factors affecting organic cation adsorption on some silicate minerals, J Colloid Interface Sci. 281 (2005) 33–38.
[5] M. Roulia, A.A. Vassiliadis, Sorption characterization of a cationic dye retained by clays and perlite, Micropor. Mesopor. Mater. 116 (2008) 732–740.
[6] B.K. Nandi, A. Goswami, M.K. Purkait, Removal of cationic dyes from aqueous solutions by kaolin: Kinetic and equilibrium studies, Appl. Clay Sci. 42 (2009) 583–590.
[7] B.H. Hameed, D.K. Mahmoud, A.L. Ahmad, Sorption of basic dye from aqueous solution by pomelo (*Citrus grandis*) peel in a batch system, Colloid Surf. A 316 (2008) 78–84.
[8] E. Demirbas, M. Kobya, M.T. Sulak, Adsorption kinetics of a basic dye from aqueous solutions onto apricot stone activated carbon, Bioresource Technol. 99 (2008) 5368–5373.
[9] B. Karagozoglu, M. Tasdemir, E. Demirbas, M. Kobya, The adsorption of basic dye (Astrazon Blue FGRL) from aqueous solutions onto sepiolite, fly ash and apricot shell activated carbon: kinetic and equilibrium studies, J. Hazard. Mater. 147 (2007) 297–306.
[10] H. Lata, V.K. Garg, R.K. Gupta, Removal of a basic dye from aqueous solution by adsorption using *Parthenium hysterophorus*: an agricultural waste, Dyes Pigments 74 (2007) 653–658.
[11] B.H. Hameed, F.B.M. Daud, Adsorption studies of basic dye on activated carbon derived from agricultural waste: *Hevea brasiliensis* seed coat, Chem. Eng. J. 139 (2008) 48–55.
[12] J.X. Lin, S.L. Zhan, M.H. Fang, X.Q. Qian, H. Yang, Adsorption of basic dye from aqueous solution onto fly ash, J. Environ. Manage. 87 (2008) 193–200.
[13] L. Margulies, H. Rozen, A. Nir, Model for competitive adsorption of organic cations on clays, Clays Clay Miner. 36 (1988) 270–276.
[14] M.A. Al-Ghouti, M.A.M. Khraisheh, M.N. Ahmad, S.J. Allen, Microcolumn studies of dye adsorption onto manganese oxides modified diatomite, J. Hazard. Mater. 146 (2007) 316–327.
[15] M. Nachtegaal, D.L. Sparks, Effect of iron oxide coatings on zinc sorption mechanisms at the clay–mineral/water interface, J Colloid Interface Sci. 276 (2004) 13–23.
[16] K.G. Bhattacharyya, S.S. Gupta, Kaolinite, montmorillonite, and their modified derivatives as adsorbents for removal of Cu(II) from aqueous solution, Sep. Purif. Technol. 50 (2006) 388–397.
[17] M.M. Mohamed, I. Othman, R.M. Mohamed, Synthesis and characterization of $MnOx/TiO_2$ nanoparticles for photocatalytic oxidation of indigo carmine dye, Photochem. Photobiol. A 191 (2007) 153–161.
[18] E. Eren, B. Afsin, Y. Onal, Removal of lead ions by acid activated and manganese oxide-coated bentonite, J. Hazard. Mater. 161 (2–3) (2009) 677–685.
[19] E. Eren, Removal of copper ions by modified Unye clay Turkey, J. Hazard. Mater. 159 (2008) 235–244.
[20] R. Dohrmann, Cation exchange capacity methodology. I: an efficient model for the detection of incorrect cation exchange capacity and exchangeable cation results, Appl. Clay Sci. 34 (2006) 31–37.
[21] N-A.M. Deraz, Physicochemical properties and catalytic behavior of magnesia supported manganese oxide catalysts, Thermochim. Acta 421 (2004) 171–177.
[22] I.F. Mironyuk, V.M. Gunko, M.O. Povazhnyak, V.I. Zarko, V.M. Chelyadin, R. Leboda, J. Skubiszewska-Zieba, W. Janusz, Magnesia formed on calcination of $Mg(OH)_2$ prepared from natural bischofite, Appl. Clay Sci. 252 (2006) 4071–4082;
I. Langmuir, The adsorption of gases on plane surfaces of glass, mica and platinum, J. Am. Soc. 40 (1918) 1361–1403.
[23] H. Freundlich, Über die adsorption in lösungen, Zeitsch. Phys. Chem. (Leipzig) 57 (1906) 385–470.
[24] S. Lagergren, About Kungliga Svenska Vetenskapsakademiens Handlingar 24 (4) (1898) 1–39.
[25] Y.S. Ho, G. McKay, Comparative sorption kinetic studies of dye and aromatic compounds onto fly ash, J. Environ. Sci. Heal. A 34 (1999) 1179–1204.
[26] W.J. Weber, J.C. Morris, J. Sanit. Eng. Div. Am. Soc. Civil Eng. 89 (1963) 31–60.
[27] M. Dogan, M. Alkan, O. Demirbas, Y. Ozdemir, C. Ozmetin, Adsorption kinetics of maxilon blue GRL onto sepiolite from aqueous solutions, Chem. Eng. J. 124 (2006) 89–101.
[28] D.M. Manohar, B.F. Noeline, T.S. Anirudhan, Adsorption performance of Al-pillared bentonite clay for the removal of cobalt(II) from aqueous phase, Appl. Clay Sci. 31 (2006) 194–206.
[29] D. Zhao, J. Zhou, N. Liu, Surface characteristics and photoactivity of silver-modified palygorskite clays coated with nanosized titanium dioxide particles, Mater. Charact. 58 (2007) 249–255.
[30] K.G. Bhattacharyya, S.S. Gupta, Adsorption of Fe(III) from water by natural and acid activated clays: studies on equilibrium isotherm, kinetics and thermodynamics of interactions, Adsorption 12 (2006) 185–204.
[31] G. Szöllösi, A. Mastalir, M. Bartok, Effect of ion exchange by an organic cation on platinum immobilization on clays, React. Kinet. Catal. Lett. 74 (2001) 241–249.
[32] G.J. Churchman, W.P. Gates, B.K.G. Theng, G. Yuan, Clays and clay minerals for pollution control, in: F. Bergaya, B.K.G. Theng, G. Lagaly (Eds.), Handbook of Clay Science, Elsevier, Amsterdam, 2006, pp. 625–675.
[33] G. Lagaly, M. Ogawa, I. Dékány, Clay mineral-organic interactions, in: F. Bergaya, B.K.G. Theng, G. Lagaly (Eds.), Handbook of Clay Science, Elsevier, Amsterdam, 2006, pp. 309–377.
[34] C.B. Hedley, G. Yuan, B.K.G. Theng, Thermal analysis of montmorillonites modified with quaternary phosphonium and ammonium surfactants, Appl. Clay Sci. 35 (2007) 180–188.
[35] P. Balaz, A. Alacova, J. Briancin, Sensitivity of Freundlich equation constant $1/n$ for zinc sorption on changes induced in calcite by mechanical activation, Chem. Eng. J. 114 (2005) 115–121.
[36] Y. El Mouzdahir, A. Elmchaouri, R. Mahboub, A. ElAnssari, A. Gil, S.A. Korili, M.A. Vicente, Interaction of stevensite with Cd^{2+} and Pb^{2+} in aqueous dispersions, Appl. Clay Sci. 35 (2007) 47–58.
[37] Y.S. Al-Degs, M.I. El-Barghouthi, A.A. Issa, M.A. Khraisheh, G.M. Walker, Sorption of Zn(II), Pb(II), and Co(II) using natural sorbents: equilibrium and kinetic studies, Water Res. 40 (2006) 2645–2658.
[38] B.H. Hameed, A.L. Ahmad, K.N.A. Latif, Adsorption of basic dye (methylene blue) onto activated carbon prepared from rattan sawdust, Dyes Pigments 75 (2007) 143–149.
[39] S. Senthilkumaar, P. Kalaamani, C.V. Subburaam, Liquid phase adsorption of Crystal violet onto activated carbons derived from male flowers of coconut tree, J. Hazard. Mater. B136 (2006) 800–808.
[40] C.-K. Lee, S.-S. Liu, L.-C. Juang, C.-C. Wang, K.-S. Lin, M.-D. Lyu, Application of MCM-41 for dyes removal from wastewater, J. Hazard. Mater. 147 (2007) 997–1005.
[41] S. Chakraborty, S. De, S. DasGupta, J.K. Basu, Adsorption study for the removal of a basic dye: experimental and modeling, Chemosphere 58 (2005) 1079–1086.
[42] C.A. Basar, Applicability of the various adsorption models of three dyes adsorption onto activated carbon prepared waste apricot, J. Hazard. Mater. B135 (2006) 232–241.
[43] R. Dhodapkar, N.N. Rao, S.P. Pande, S.N. Kaul, Removal of basic dyes from aqueous medium using a novel polymer: Jalshakti, Bioresource Technol. 97 (2006) 877–885.
[44] Y. Onal, Kinetics of adsorption of dyes from aqueous solution using activated carbon prepared from waste apricot, J. Hazard. Mater. B137 (2006) 1719–1728.
[45] S. Wang, H. Li, L. Xu, Application of zeolite MCM-22 for basic dye removal from wastewater, J Colloid Interface Sci. 295 (2006) 71–78.
[46] A. Al-Futaisi, A. Jamrah, R. Al-Hanai, Aspects of cationic dye molecule adsorption to palygorskite, Desalination 214 (2007) 327–342.
[47] K. Porkodi, K.V. Kumar, Equilibrium, kinetics and mechanism modeling and simulation of basic and acid dyes sorption onto jute fiber carbon: eosin yellow, malachite green and crystal violet single component systems, J. Hazard. Mater. 143 (2007) 311–327.
[48] C.-H. Wu, Adsorption of reactive dye onto carbon nanotubes: equilibrium, kinetics and thermodynamics, J. Hazard. Mater. 144 (2007) 93–100.
[49] M. Chairat, S. Rattanaphani, J.B. Bremner, V. Rattanaphani, An adsorption and kinetic study of lac dyeing on silk, Dyes Pigments 64 (2005) 231–241.
[50] B.S. Inbaraj, C.P. Chiu, G.H. Ho, J. Yang, B.H. Chen, Effects of temperature and pH on adsorption of basic brown 1 by the bacterial biopolymer poly(γ-glutamic acid), Bioresource Technol. 99 (2008) 1026–1035.
[51] M. Al-Ghouti, M.A.M. Khraisheh, M.N.M. Ahmad, S. Allen, Thermodynamic behaviour and the effect of temperature on the removal of dyes from aqueous solution using modified diatomite: a kinetic study, J Colloid Interface Sci. 287 (2005) 6–13.